PAVEMENT SLABS RESTING ON ELASTIC FOUNDATION

Surendra K. Saxena, Port Authority of New York and New Jersey

The development of a rational method of analysis of any system must include the selection and analysis of a model for realistic input parameters. Based on this idea, a simple method has been developed for solution of often encountered problems of engineering practice involving slabs resting on subgrade. The slab is represented by a physical model, which is helpful in visualizing the problem and forming a solution. Regarding subgrade, most of the available analyses assume it to be a Winkler model, a physical model of a heavy liquid, or a bed of springs. In this paper the soil is treated as an elastic solid. With these two models for slab and subgrade, a computer method based on matrix analysis has been developed. From the solution of reactive subgrade pressures, the deflections are then subsequently used to compute stresses and bending moments. Two exemplary problems, one with a corner load and one with a center load, have been included. Comparison of the latter with the Winkler model is illustrated.

•MOST pavement analyses are based on the assumption that the deflection of the slab at any point is proportional to the reaction pressure at that point and does not depend on the pressure at any other point of foundation. This assumption, originating from Winkler (1), corresponds to the physical model of a heavy liquid or bed of springs.

The physical properties of the soils, however, are much more complicated than indicated by such a simple relation assumed by Winkler. From the known fact that soils can propagate waves, it is obvious that they can behave closer to elastic solids than to beds of springs. Wieghart (2) was the first to investigate the analogous beam problem under the general assumption that the deflection at any point depends on the subgrade reactions along a certain length 2L of the subgrade:

$$y(x) = \text{const.} \int_{-L}^{+L} g(\xi)k(|x - \xi|)d\xi \qquad (1)$$

where

y = deflection of a beam,
g = subgrade reaction,
k = a kernel function depending on type of subgrade.

Several investigators (3-8) developed solutions for different kernels, k, mostly through the use of Fourier integrals. However, no kernel function of space coordinates could reproduce the exact actual behavior of the subgrade. With the knowledge of soil behavior, the investigators have, of late, tried to include a function of time in the relation between deflection and reaction pressure. Ideally, such a model will be a nearly true representative of soil subgrade; its application has been very limited because of the rigorous mathematics involved.

Publication of this paper sponsored by Committee on Theory of Pavement Design.

In the particular case of a thin slab of infinite extent, exact solutions have been provided by Hogg (9) and Holl (10) by using elastic solid subgrade. Burmister (11), treating both the slab and the subgrade as elastic isotropic solids, has proceeded from the three-dimensional general equations of elasticity to find the solutions for a two- or three-layered solid. His work, however, deals with slabs of infinite extent only. Circular slabs of limited dimensions have been dealt with by Habel (12), who used difference methods. Other specific cases of slabs of finite dimensions have been investigated by De Beer (13), Grasshoff (14), Schultze (15), Kany (16), and Krasmanovic (17). A summary of extensive Russian studies along similar lines has been completed by Vlassov and Leont'ev (18).

Because of the rigor of mathematics used, few of the preceding works have been adopted by practicing engineers as regular tools in analysis. Limited solutions suitable for practical use aimed at load distributions over only circular loading surfaces have been developed (19, 20) where the influence values for a load on the interior of a slab have been calculated according to Hogg (elastic solid subgrade), but the edge loads have been computed according to Westergaard (Winkler subgrade). This work was subsequently extended by Pickett, Badaruddin, and Ganguli (21) to include the case of semi-infinite slab.

In the present paper, based on thin-plate theory, a physical model of the slab has been adopted. The model can handle homogeneous as well as orthotropic slabs of variable thickness. The subgrade is represented by an elastic, isotropic, homogeneous solid of infinite extent with a modulus of elasticity E_s and Poisson's ratio ν_s.

PHYSICAL MODEL OF THE SLAB

The finite-element model of the slab in this study was developed after Newmark by Hudson and Matlock (22). Figure 1 shows a typical nodal point. The axial deformability and Poisson's effects of slab elements are represented by elastic blocks. The torsional stiffness of the elements is represented by torsion bars and is always active in the system. It should be noted that the slab so formed may be of orthotropic behavior in any single element. There may be also arbitrary differences in individual stiffnesses of different elements. The free-body diagram of a nodal point giving all internal forces of the system is shown in Figure 2.

In the Hudson-Matlock model, the reaction of the subgrade was represented by a spring, giving it Winkler qualities. In the present study, the subgrade is treated as an isotropic elastic solid, and the reaction of the subgrade is represented by a force under the nodal point. This reactive force under node affects the whole continuum (elastic solid) and consequently influences all the forces and displacements of the continuum. The real difficulty experienced in the use of this subgrade is to account for all these influences. With the help of computers, it has been accomplished by superposition, by using Boussinesq's solution and Maxwell's reciprocal relation.

FORMULATION OF EQUATIONS

The equation of vertical equilibrium of a nodal point can be written as

$$-Q_{i,j} + S_{i,j} = V^x_{i,j} + V^y_{i,j} - V^x_{i+1,j} - V^y_{i,j+1} \qquad (2)$$

The shearing forces V in this expression can be evaluated in terms of bending and twisting moments that, in turn, can be expressed by their finite difference equivalents in terms of deflections of adjacent points.

After all transformations, Eq. 2 appears as a linear equation containing an unknown deflection of 13 nodal points clustered in a rhomboidal array around the considered nodal point i, j. It can be represented in matrix form as

$$[K_p]\{W\} = -\{Q\} + \{P\} \qquad (3)$$

Figure 1. Typical joint i with j taken from finite-element slab model (22).

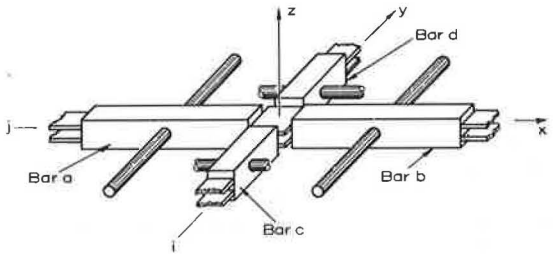

Figure 2. Free body of slab mesh point.

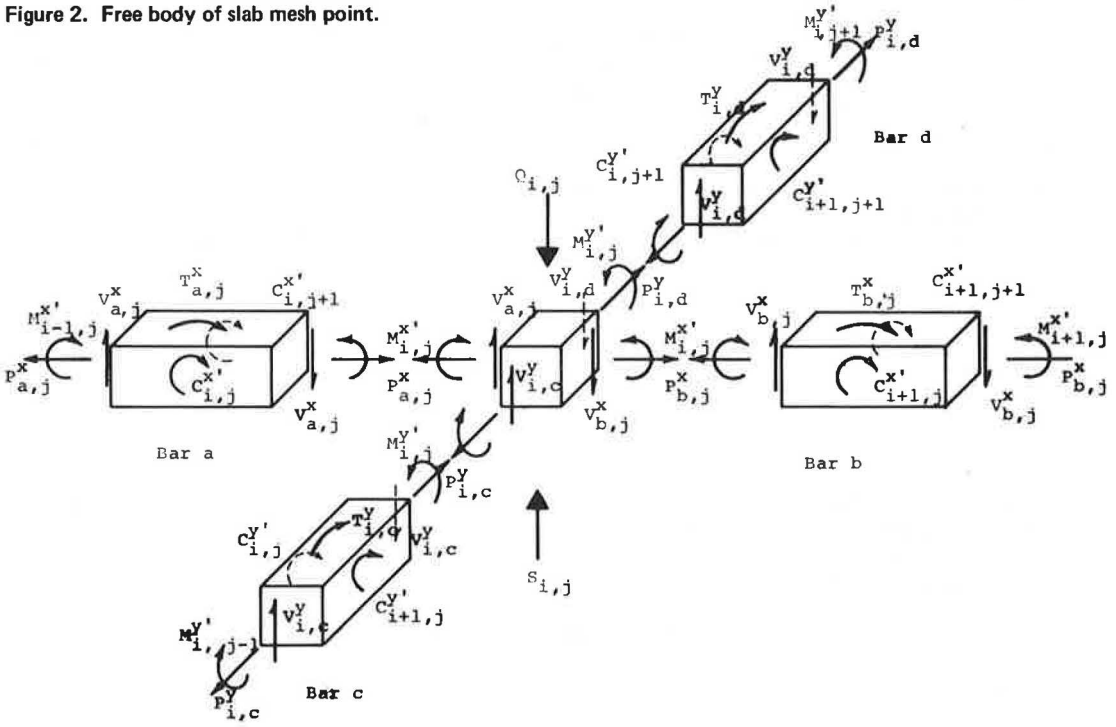

where

$[K_p]$ is termed as stiffness matrix of slab,
$\{W\}$ is deflection matrix,
$\{Q\}$ is load matrix, and
$\{P\}$ is reaction matrix.

Because we are using the finite-difference equations for moments, the stiffness matrix so obtained utilized one fictitious station beyond the real boundary of the slab. At those points, the terms in the load and reaction matrices are zero; i.e., the right-hand side of Eq. 3 is equal to zero. If the equations at these points were written, it would be immediately clear that they represent the so-called Kirchoff's conditions of the bending moments, being zero at edges. Figure 3 shows the forms of the K_p, W, Q, and P matrices.

The matrix $[K_p]$ and W can be rearranged as follows:

$$\begin{bmatrix} K_p^1 & K_p^2 \\ \hline K_p^3 & K_p^4 \end{bmatrix} \begin{Bmatrix} W_e \\ \hline W_i \end{Bmatrix} = \begin{Bmatrix} 0 \\ \hline -Q \end{Bmatrix} + \begin{Bmatrix} 0 \\ \hline P \end{Bmatrix} \tag{4}$$

where

$\{W_e\}$ represents deflections of all points external to real slab boundary, i.e., the fictitious points used; and
$\{W_i\}$ represents all internal points, i.e., points within real slab boundary.

Equation 4 can then easily be split into two as follows:

$$[K_p^1]\{W_e\} + [K_p^2]\{W_i\} = 0 \tag{5}$$

and

$$[K_p^3]\{W_e\} + [K_p^4]\{W_i\} = -\{Q\} + \{P\} \tag{6}$$

Equation 5 can furnish W_e in terms of W_i so as to satisfy the bending moments at boundaries to be zero. It may, however, be noted that the deflections W_e are not real because the slab does not exist there. They are used only to satisfy the boundary conditions in terms of finite differences. Consequently, from Eq. 5

$$\{W_e\} = -[K_p^1]^{-1}[K_p^2]\{W_i\} \tag{7}$$

Substituting this value of W_e in Eq. 6

$$-[K_p^3][K_p^{12}]\{W_i\} + [K_p^4]\{W_i\} = -\{Q\} + \{P\} \tag{8}$$

where

$$[K_p^{12}] = [K_p^1]^{-1}[K_p^2] \tag{9}$$

Naming

$$[BK_p] = [K_p^3][K_p^{12}] \tag{10}$$

one gets

$$\left[[K_p^4] - [BK_p]\right]\{W_i\} = -\{Q\} + \{P\} \tag{11}$$

Finally, calling

$$[AK_p^4] = [K_p^4] - [BK_p]$$

the simplified form of the equation becomes

$$[AK_p^4]\{W_1\} = -\{Q\} + \{P\} \tag{12}$$

This equation utilizes only the points within the real boundary of the slab and also serves to satisfy the boundary conditions.

FLEXIBILITY MATRIX OF SUBGRADE

It can be noted in Eq. 12 that matrix $[AK_p^4]$ is known and $\{Q\}$ is known, but the terms of matrices $\{W_1\}$ and $\{P\}$ are both unknown. Consequently the necessity of expressing the relation between $\{W_1\}$ and $\{P\}$ becomes obvious.

For an elastic isotropic solid, the deflection due to unit vertical and horizontal point loads has been given by Boussinesq and Cerruti. According to them the deflection at any point B due to a point load A is given as

$$W_{BA} = \frac{P}{\pi d_s} \frac{(1 - \nu_s^2)}{E_s} \tag{13}$$

where

P = load at point A, and
d_s = radial distance between points A and B.

Other terms have been previously explained. From Eq. 13, the deflection at the center of a uniformly loaded rectangular area (a × b) can be obtained by integration (Fig. 4):

$$W_1 = 2 \int_0^{x=a/2} \int_0^{y=b/2} \frac{P}{ab} \frac{(1 - \nu_s^2)}{\pi E_s} \frac{dx\,dy}{\sqrt{x^2 + y^2}} = \frac{P}{b} \frac{(1 - \nu_s^2)}{\pi E_s} I_w \tag{14}$$

where I_w for the case a = b equals 3.525. The value of I_w for cases commonly found are a/b = 2, I_w = 2.406; a/b = 3, I_w = 1.867; a/b = 4, I_w = 1.543; and a/b = 5, I_w = 1.322.

For any point outside the loaded area, one can do similar integration, but very good approximation can be achieved only by using Eq. 13 (by taking P as total load over the rectangle and d_s as center to center distance). Zienkiewicz (24) compared some exact results with that from Eq. 13 and found that, even for x = a, the error is only some 4 percent and decreases rapidly with increase of x.

Hence, using any set of grid points, in the case when the subgrade is of infinite depth, the deflections can be written as

$$W = -\frac{(1 - \nu_s^2)}{\pi E_s b} [f_f]\{P\} \tag{15}$$

where $[f_f]$ is the flexibility matrix of the foundation and can be obtained by Eq. 13 for points off the loaded area and by Eq. 14 for points under the loaded area.

COUPLING THE STIFFNESS MATRIX OF SLAB AND FLEXIBILITY MATRIX OF SUBGRADE

The column matrix W discussed previously is formed by the deflections of the interior points of any real slab and is thus analogous to the column matrix W_1 of Eq. 12. Substituting therefore the value of W from Eq. 15 into Eq. 12, one gets

$$[AK_p^4][AF_f]\{P\} = -\{Q\} + \{P\} \tag{16}$$

where

$$[AF_f] = -\frac{(1 - \nu_s^2)}{\pi E_s a}[f_f] \tag{17}$$

or

$$\left[[AK_p^4][AF_f] - I\right] \times \{P\} = -\{Q\}$$

where I is an identity matrix or

$$\{P\} = \left[[AK_p^4][AF_f] - I\right]^{-1} \{-Q\} \tag{18}$$

Having known $\{P\}$, we can find the deflections from Eq. 15. By using this approach, it is not necessary to invert the matrix $[AF_f]$. In all, two inversions are involved in the whole process, one being the inversion of matrix $[K_p^1]$ that will invariably be a small matrix and the other being inversion of a large matrix (size equal to number of increments in x-direction multiplied by number of increments in y-direction), $\left[[AK_f^4][AF_f] - I\right]$.

PROBLEM EXAMPLES

For illustration, two problems have been selected. The first case is a square slab with corner load, and the second one is with a center load.

Square Slab With Corner Load

The problem has been analyzed for different values of a nondimensional flexibility number

$$\alpha = \frac{E_s b a^3}{EI}$$

where

b = breadth of slab,
a = length of slab,
I = moment of inertia per unit width of slab,
E = modulus of slab, and
E_s = modulus of subgrade.

A larger value of α indicates a more flexible slab and vice versa.

Figure 5 shows a square slab in plan with many lines, each identified by a flexibility number. The two edges 1-2 and 1-4, and each one of these lines, represent the area of contact of the slab with subgrade, when the point of application of load is point 1.

Westergaard's corner formula has been investigated by many workers. According to it, the numerically greatest value of bending moment per unit widths is given by

$$M = -\frac{Q}{2}\left\{1 - \left(\frac{a_1}{1_0}\right)^{0.6}\right\} \tag{19}$$

where

$a_1 = r\sqrt{2}$, and
r = the diameter of area on which the load is acting.

This bending moment M occurs approximately at a distance

$$x_1 = 2\sqrt{a_1}\, 1_0 \tag{20}$$

from the load $\left[1_0 = \text{radius of relative stiffness} = \sqrt[4]{\frac{Et^5}{12(1 - \nu)k}}\right]$

Figure 3. Form of K, W, Q, and P matrices.

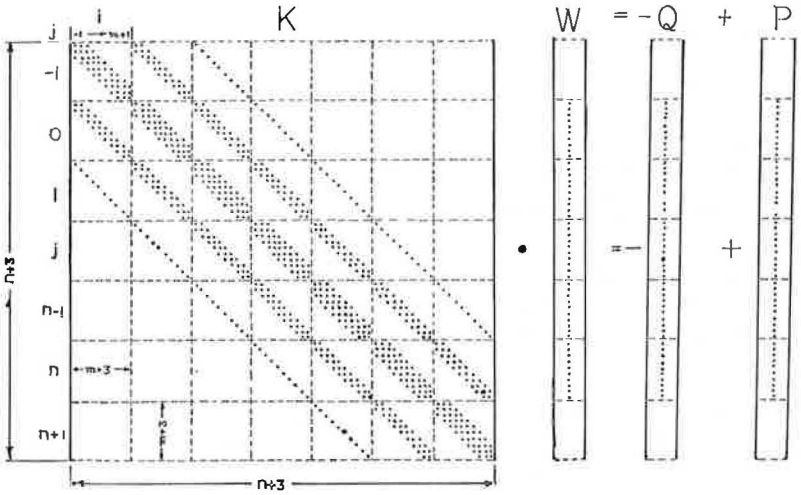

Figure 4. Deflection due to a uniformly loaded slab on isotropic solid subgrade.

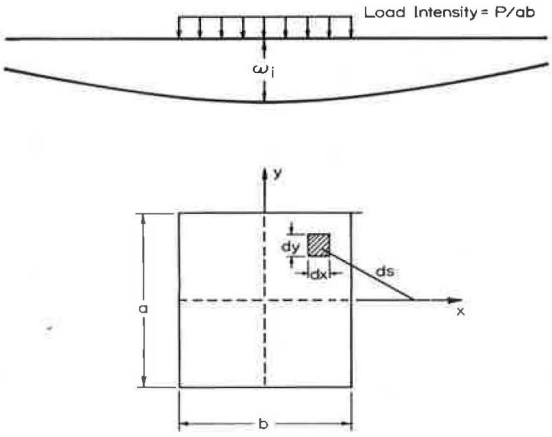

Figure 5. Lines of separation of contact with subgrade.

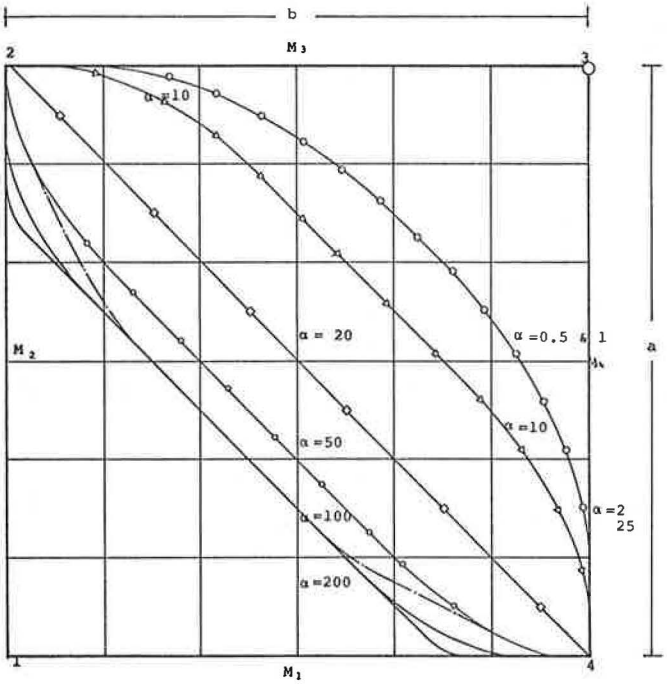

In cases where r = 0, a_1 will automatically become zero. The maximum moment becomes equal to $-\frac{Q}{2}$ and, according to formula, should occur under the load. This result that, regardless of the stiffness of slab and modulus of subgrade, the maximum bending moment will always be $-\frac{Q}{2}$ does not seem correct.

Investigations were therefore done for a point load applied at a corner of slabs of different rigidities. Figures 5 through 12 show the results of investigations. From Figure 7, it appears that the maximum moment along the diagonal changes in magnitude as well as location with the α-value. The peak moment is nearer to the point of application of load in case of flexible slabs and is farther for rigid slabs. The magnitude also increases with rigidity. Table 1 gives the results of investigations. The maximum bending moments due to Westergaard's considering the load as point load have been computed. Also computed are the bending moments, when the load is considered to be uniformly spread over a circle of radius r such that

$$\pi r^2 = (h_x/4) \times (h_y/4)$$

It was also revealed that, if the value of α is plotted on log scale against the distance of peak points from the point of load application, the points fall on a straight line. Figure 9 shows such a plot. From the figure one can get the relation

$$d_1 = d \left\{0.083 + 0.0765 \left(\log \frac{330}{\alpha}\right)\right\} \qquad (21)$$

where

d = diagonal of square slab, and
d_1 = distance of maximum moment point from corner where load is applied.

It was also found that if α is plotted on log scale against magnitude of maximum bending moments, the points fall on one straight line. Figure 10 is a plot of this type and gives the following relation

$$M_{max} = Q \left(0.21 + 0.0215 \log \frac{420}{\alpha}\right) \qquad (22)$$

It may be pointed out that, for values of α less than 2, the preceding relations do not hold, though they will not be far off.

For a slab with a corner load, this is a significant relation that relates the moments to the relative flexibility number and has been derived for the first time.

Square Slab With Center Load

This example compares the results obtained from an elastic solid model with that of a Winkler model. This comparison was part of a model test (performed under controlled conditions) to study the effect on stresses due to load alone (25).

An aluminum slab 2 ft sq and ½ in. thick was used. The ratio between thickness and length in this test was 1:48, whereas in actual pavements it ranges from 1:40 to 1:80. The modulus of elasticity of aluminum used is 10.5×10^6 psi, and its Poisson's ratio is 0.33. The loads were applied through a 4-ton hydraulic jack, in equal increments. The maximum load was well below the ultimate load that could cause yield in slab. A yellow silty clay with a maximum dry density of 111 lb/ft^3 at optimum moisture content of 16 percent was used as soil model.

Loads were recorded by a calibrated proving ring, and strain gauges were used to read strains at various slab locations. For deflection measurements, dial gauges were utilized. Figure 13 shows the setup, and Figure 14 shows the plan of slab with position of dial and strain gauges.

Figure 6. Pressure distributions along edge of square slab loaded at corner.

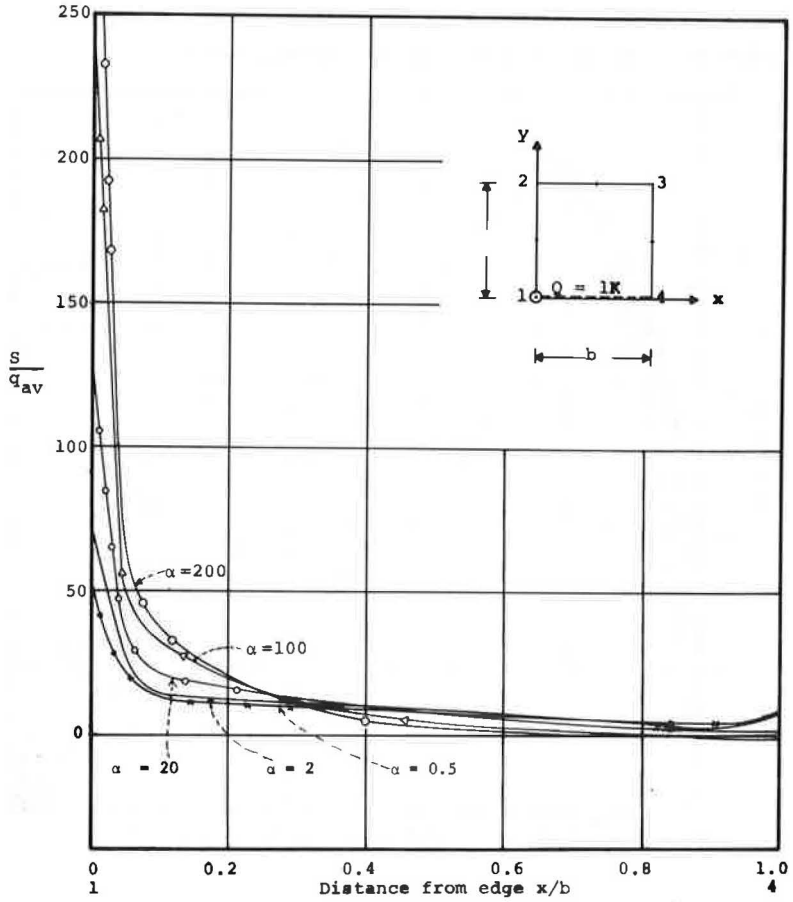

Figure 7. Bending moment along diagonal of square slab loaded at corner.

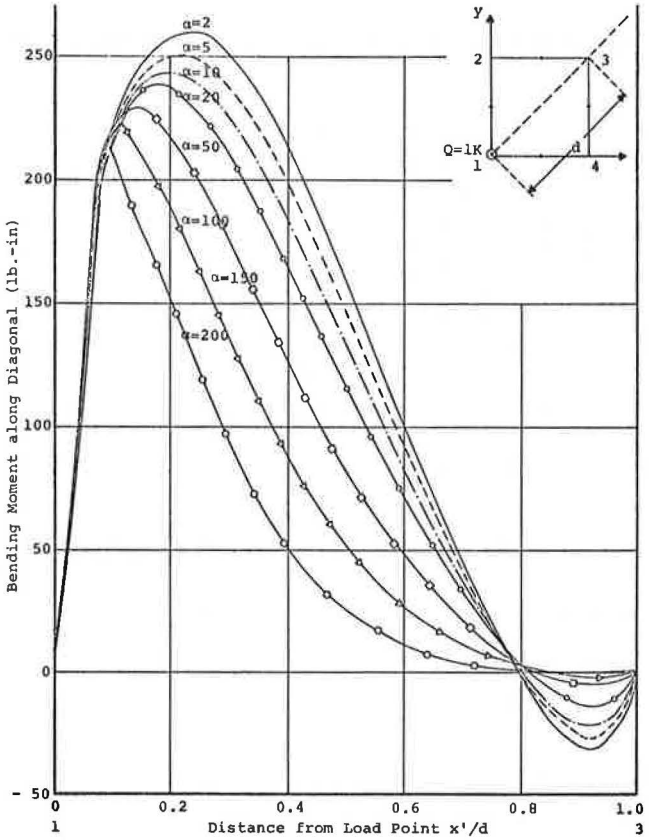

Figure 8. Bending moment along edge of slab loaded at corner.

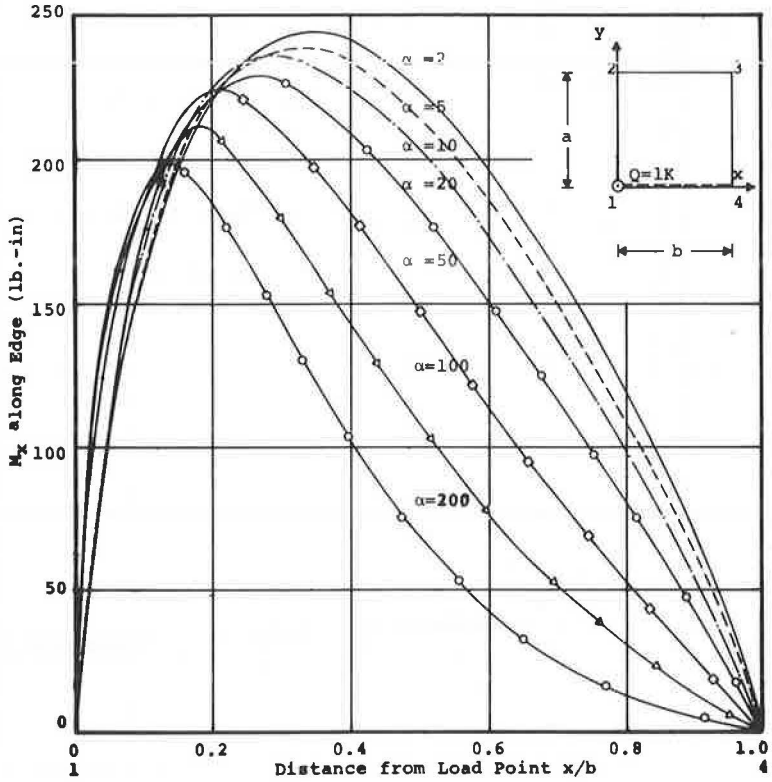

Figure 9. Relation of location point of maximum stress and flexibility number for corner load.

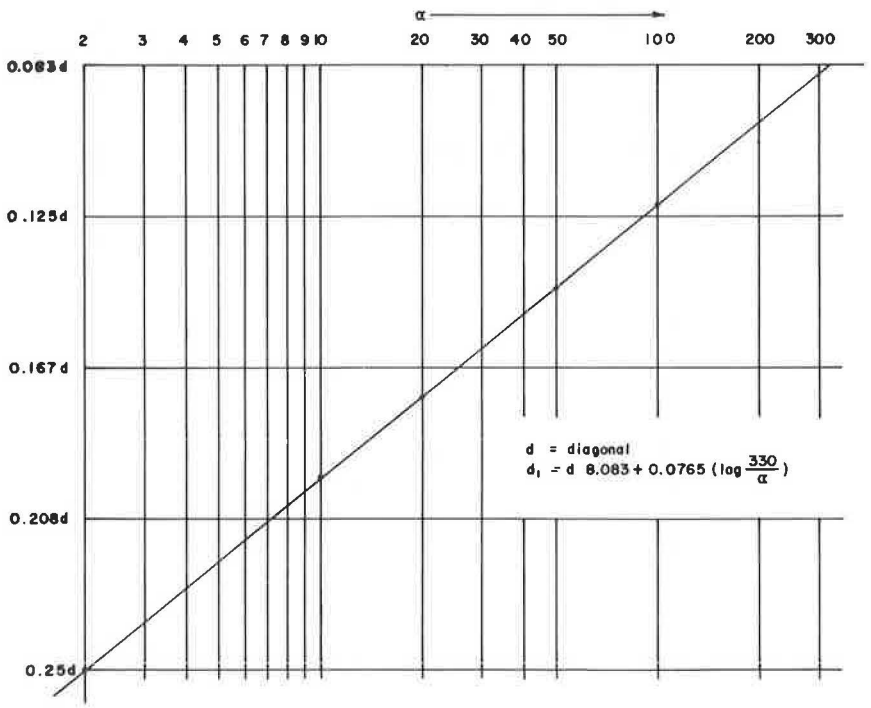

Figure 10. Relation of maximum bending moment and flexibility number for corner load.

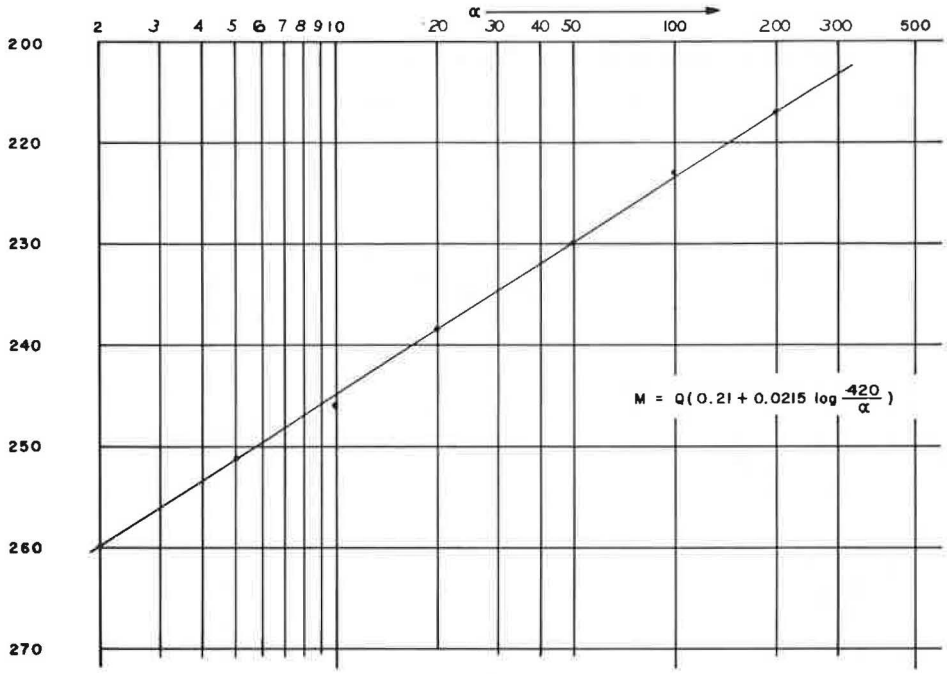

Figure 11. Deflection along edge of square slab loaded at corner.

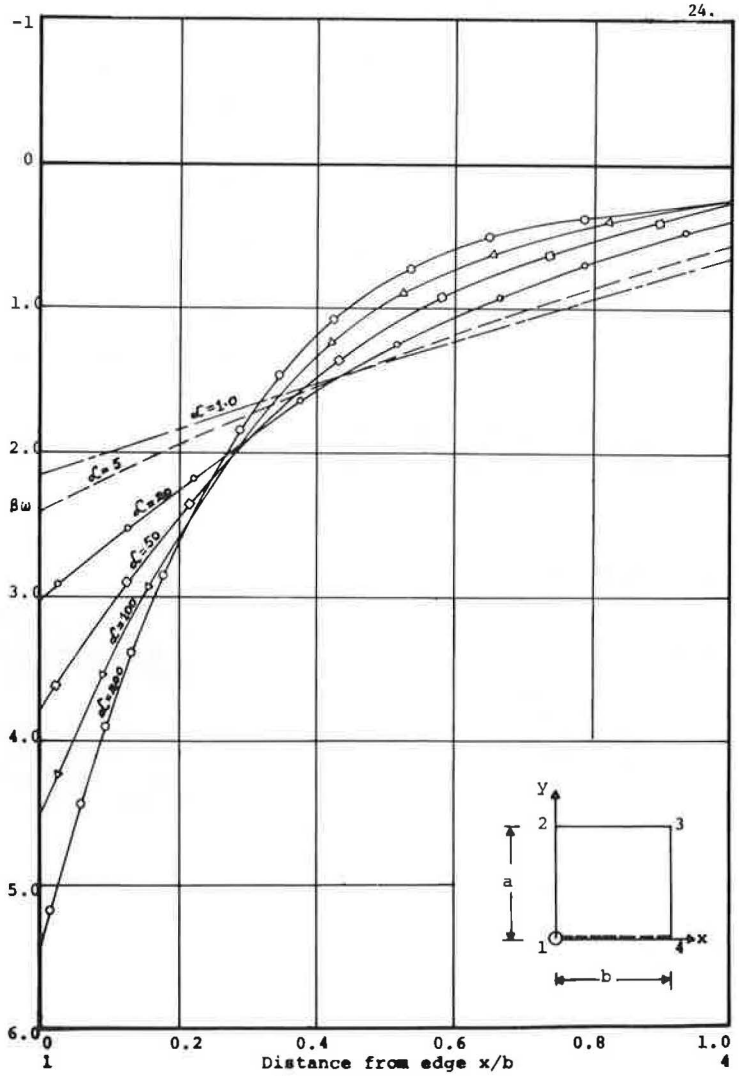

Figure 12. Deflection along diagonal of square slab loaded at corner.

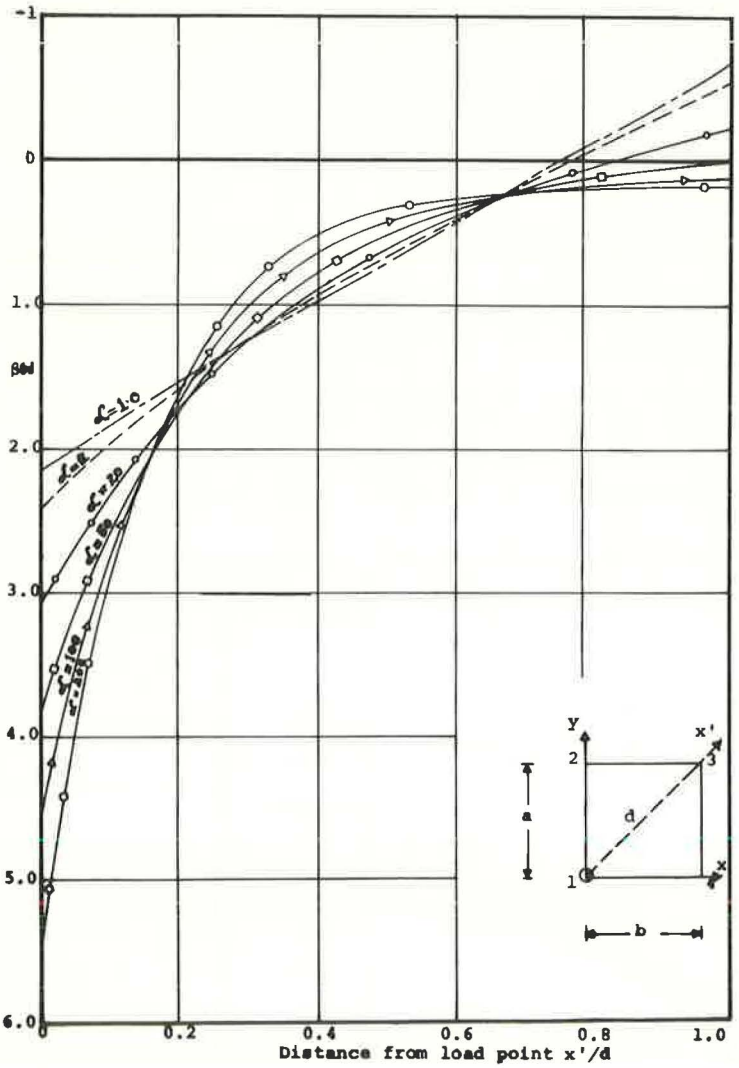

Table 1. Maximum moments in square slab with corner load.

Flexibility Number	Maximum Moments, Westergaard (lb-in.)		Maximum Moments, Elastic Solid Subgrade (lb-in.)
	With Point Load	With Load Spread on $\left(\frac{h_x}{4} \times \frac{h_y}{4}\right)$	
2	500	444	260
5	500	433	251
10	500	423	246
20	500	411	239
50	500	394	230
100	500	378	222
200	500	360	212

Figure 13. Test equipment.

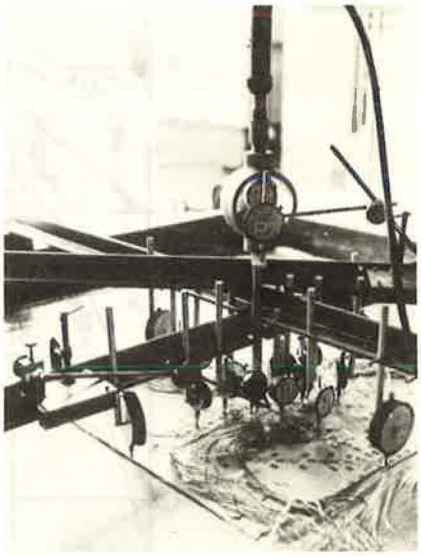

The modulus value of the soil was computed from the measured deflection bowl by the following formula developed by Losberg (26):

$$E_s = [\theta t E^{1/3} (1 - \nu_s^2)]^{3/4}$$

where

t = the thickness of slab,
E = modulus of elasticity of slab, and
θ = slope of load versus depression volume curve.

The value of E_s obtained was 1,550 psi.

Figure 15 shows the deflections. The results show that the values of deflection computed from Westergaard's formula and those from discrete-element model using Winkler subgrade are comparable. These values differ from the elastic solid subgrade though the patterns are very nearly the same. The deflection computed from the discrete-element model using elastic solid subgrade shows remarkable agreement with observed deflections.

From Figure 16, one can see that the observed stresses and those computed by using both Winkler subgrade and elastic solid subgrade are very nearly the same except at maximum point. The difference between observed stresses and those computed by elastic solid theory is about 8 percent. The difference between the observed stresses and those computed using Winkler subgrade is 21 percent. The stresses were computed by Westergaard's formula as well, and the difference between the observed and Westergaard's is about 40 percent. The stresses according to Westergaard's formula are for an infinite slab and a Poisson's ratio of 0.15, whereas the value used in other computations was 0.33. The k-value used in Westergaard's formula was computed from the following:

$$k = \frac{1}{t} (E_s/E^{1/3}) [E_s/(1 - \nu_s^2)]$$

The relevant results are maximum center load, 3,953 lb; maximum observed stress, 20,750 psi; maximum theoretical stress (Westergaard), 31,625 psi; maximum theoretical stress (Winkler), 25,110 psi; maximum theoretical stress (elastic solid), 22,400 psi; maximum observed deflection, 0.180 in.; maximum theoretical deflection (Winkler), 0.123 in.; and maximum theoretical deflection (elastic solid), 0.1825 in.

CONCLUSIONS AND RECOMMENDATIONS

A simple method for solutions of often encountered problems of engineering practice, involving slabs resting on an elastic solid subgrade, has been developed. The slab model utilized is a discrete model developed by Hudson and Matlock (22). The discrete model allows the use of two-dimensional structural elements to represent a thin slab, and the behavior of the elements of assembly of different structural elements forming the slab can be described by algebraic equations. The model is not equivalent to the exact one, but can be made as accurate as desired.

Two illustrative examples have been presented. For the case of square slab with corner load, it is found that the location and the magnitude of peak moments change with the rigidity of slab. Simple expressions for predicting the location as well as magnitude of maximum moments are furnished.

In the second problem, an experimental investigation has been compared with various theoretical soil models. It was found that results from Westergaard's formula agree closely with that of Winkler model and that the elastic solid model simulated the actual behavior better.

When the subgrade is not an elastic half-space but is made up of layers of different materials with different moduli of elasticity and Poisson's ratios, the case becomes more complicated. The deflection of a slab of finite dimensions, resting on elastic layers, has not yet been solved. Steinbrenner (27) has worked an approximate solution

Figure 14. Plan of slab with position of gauges.

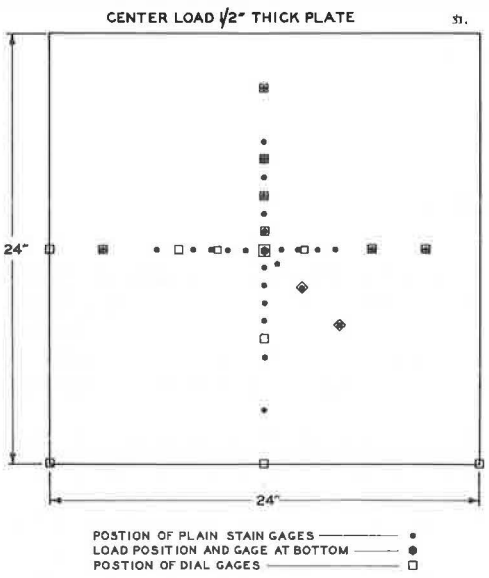

Figure 15. Stress along centerline of ½-in. thick slab.

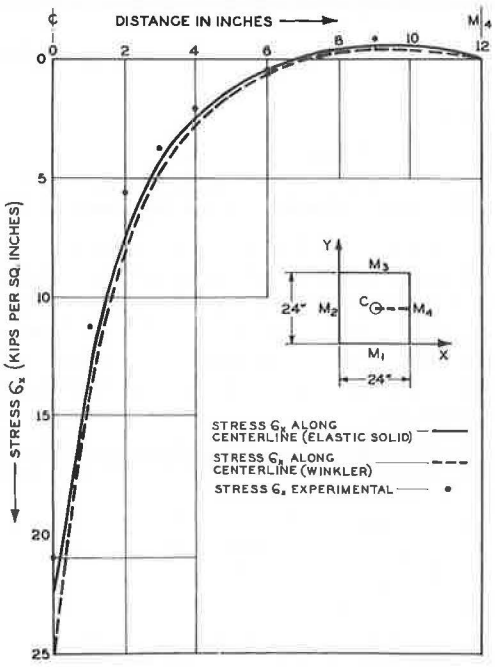

Figure 16. Deflection profile of ½-in. thick slab.

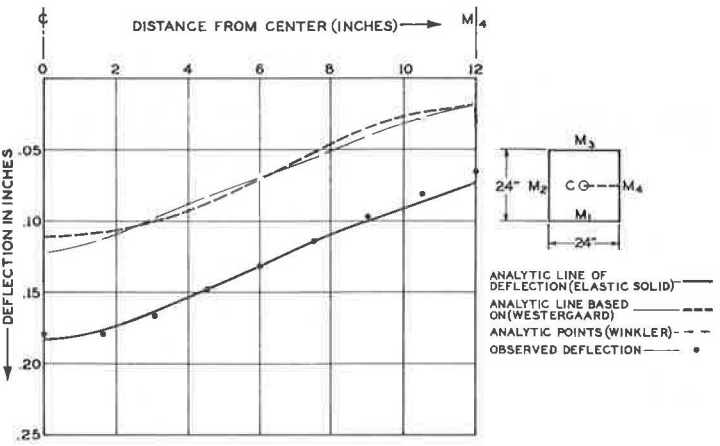

that, according to Terzaghi, is accurate enough for practical purposes. Extension of the work to account for three layers of soil has been completed by Saxena (25).

ACKNOWLEDGMENTS

The valuable guidance and help in this analytical work from A. S. Vesic of Duke University is gratefully acknowledged.

The assistance of Margo Downey, who typed the manuscript, is appreciated.

The encouragement of the Port Authority of New York and New Jersey by providing facilities is deeply appreciated.

REFERENCES

1. Winkler, E. Die Lehre von der Elastizitat und Festigkeit. Prague, 1867, p. 182.
2. Wieghart. Ueber den Balken auf nachgiebiger Unterlage. ZAMN, Vol. 2, 1922, pp. 165-184.
3. Prager, W. Zur Theorie elastisch gelagerter Construktionen. ZAMN, Vol. 7, 1927, pp. 354-360.
4. Nemenyi, P. Tragwerke auf elastisch nachgiebiger Unterlage. ZAMN, Vol. 2, 1931, pp. 224-231.
5. Marguerre, K. Ueber den Traeger auf elastischer Unterlage. ZAMN, Vol. 17, 1937, pp. 224-231.
6. Biot, M. A. Bending of an Infinite Beam on an Elastic Foundation. Trans. ASME, Vol. 59, PPA1-A7, 1937.
7. Reissner, E. On the Theory of Beams Resting on a Yielding Foundation. Proc. National Academy of Sciences, Vol. 23, 1937, pp. 328-333.
8. Volterra, E. Sul Problema Generale della trave poggiata su suolo elastico. Rend. Acad. Nazionale die Lincei, Vol. 2, Series 8, 1947, pp. 307-311, 418-421.
9. Hogg, A. H. A. Equilibrium of a Thin Slab on Elastic Foundations of Finite Depths. Phil. Magazine, Vol. 35, 1944, pp. 265-276.
10. Holl, D. L. Thin Plates on Elastic Foundations. Proc. 5th Internat. Congress on Applied Mechanics, Cambridge, Mass., 1938.
11. Burmister, D. M. The General Theory of Stresses and Displacements in Layered Systems. Jour. Applied Physics, Vol. 16, Feb., March, May 1945.
12. Habel, A. Die auf dem elastisch-isotropen Halbraumn aufruhende zentral symmetrisch belastete elastische Kreisplatte. Bauing, Vol. 18, 1937.
13. De Beer, E. E., Lousberg, E., and Van Beveren, P. Le Calcul de poutres et plaques appuyées sur le sol. Annales des travaux publics de Belgique, No. 2-3, 1956.
14. Grasshoff, H. Die Berechnung einachsig Ausgesteifter Grundungsplatten. Bautechnik, Vol. 32, p. 396. (See also Influence of Flexural Rigidity of Superstructure on Distribution of Contact Pressure and Bending Moments of an Elastic Combined Footing. Proc. 4th Internat. Conf. on Soil Mechanics and Foundation Engineering, London, Vol. 1, pp. 300-356.)
15. Schultze, E. Distribution of Stress Beneath a Rigid Foundation. Proc. 5th Internat. Conf. on Soil Mechanics and Foundation Engineering, 1961, pp. 807-813.
16. Kany, M. Berechnung von Flachengrundungen. Verlag and Ernst und Sohn, Berlin.
17. Krasmanovic, D. Influence de la continuité et de la rigidité sur le calcul des constructions et des poutres continues de foundations. Annales des Travaux Publics de Belgique, Vol. 108, 1955, p. 61.
18. Vlasov and Leont'ev. Beams, Plates and Shells on Elastic Foundation. Israel Program for Scientific Translation, Jerusalem, 1966. (In Russian.)
19. Pickett, G., and Ray, G. K. Influence Charts for Concrete Pavement. Trans. ASCE, Paper 2425, Vol. 116, 1951, p. 49.
20. Pickett, G., Raville, M. E., Jones, W. C., and McCormick, F. J. Deflections, Moments and Reactive Pressure for Concrete Pavements. Kansas State College, Manhattan, Bull. 65, Oct. 15, 1951.

21. Pickett, G., Badaruddin, S., and Ganguli, S. C. Semi-Infinite Pavement Slab Supported by an Elastic Solid Subgrade. First Congress on Theoretical and Applied Mechanics, Kharagpur, India, 1955, pp. 52-60.
22. Hudson, W. R., and Matlock, H. Analysis of Discontinuous or Isotropic Pavement Slabs Subjected to Combined Loads. Center for Highway Research, Univ. of Texas at Austin, Aug. 1965.
23. Todhunter, I., and Pearson, K. A History of the Theory of Elasticity. Cambridge Univ. Press, 1893.
24. Zienkiewicz, O. C., and Cheng, Y. K. Plates and Tanks on Elastic Foundations: An Application of Finite Element Method. Internat. Jour. of Solid Structures, Vol. 1, 1965, pp. 451-461.
25. Saxena, S. K. Foundation Mats and Pavement Slabs Resting on an Elastic Foundation: Analyzed Through a Physical Model. Duke Univ., Durham, PhD dissertation, 1971.
26. Losberg, A. Structurally Reinforced Concrete Pavement. Chalmers Tekniska Hogskolas Handingar, Goteberg, dissertation, 1960.
27. Steinbrenner, W. C. Tafelen zur Setzungsberechnung. Die Strasse, Vol. 1, 1951, pp. 121-124.